J Vis (2010) 13:241–250
DOI 10.1007/s12650-010-0038-x

REGULAR PAPER

Tomasz P. Bednarz · Chengwang Lei · John C. Patterson

Various aspects of camera settings and image processing in the calibration of thermo-chromic liquid crystals for accurate particle image thermometry measurements

Received: 19 February 2009 / Accepted: 11 September 2009 / Published online: 30 April 2010

Abstract Step-by-step calibration procedures of particle image thermometry (PIT) for non-invasive and accurate temperature measurements using thermo-chromic liquid crystals (TLCs) are described in this paper. The purpose of this study is to examine the effects of various aspects of camera settings and image and data processing on the calibration of TLCs, and reveal the optimal parameter settings for achieving the best calibration curve of temperature versus color. Based on this study, an optimal window size has been proposed for median filtering to achieve the best compromise between noise removal and retaining of the true color information of the original experimental photographs; an optimal white balance settings in terms of the color temperature has been revealed for the present optical system; and finally, an optimal configuration of neural networks has been identified for obtaining the best hue–temperature correlation for further experiments.

Keywords Image processing · Median filter · Particle image thermometry

1 Introduction

Accurate temperature field data is essential for heat transfer and fluid flow analyses, especially for evaluation of convective heat transfer coefficients in complex geometries or in dynamic fluid flows. Traditional temperature sensors such as thermocouples or thermistors can only provide temperature information at discrete points; and moreover, the presence of these sensors in the flow domain may disturb the original flow. Therefore, temperature measurements based on thermo-chromic liquid crystals (TLCs) have advantages over conventional temperature sensors in that the method is non-invasive and can map the full temperature field instantaneously, provided that proper calibration process and image post-processing techniques are adopted (Fujisawa and Funatani 2000; Park et al. 2001; Smith et al. 2001).

The TLCs usually exist in smectic, nematic or cholesteric phases. When a white light source shines on the chiral nematic TLC, only the light of a particular wavelength corresponding to its temperature is reflected. The visible colors of TLCs turn from colorless to red at a given temperature, and as the temperature is increased, pass through other colors of the visible spectrum in sequence (orange, yellow, green,

T. P. Bednarz (✉)
CSIRO Earth Science and Resource Engineering, Technology Court, Pullenvale, QLD 4069, Australia
E-mail: tomasz.bednarz@csiro.au
URL: http://www.csiro.au
Tel.: +61-7-33274706
Fax: +61-7-33274566

C. Lei · J. C. Patterson
School of Civil Engineering, The University of Sydney, Sydney, NSW 2006, Australia

blue, violet) before turning colorless at a higher temperature (Smith et al. 2001). These color changes have been stated as repeatable and reversible, however, a hysteresis effect has also been reported (Anderson and Baughn 2004).

TLC sheets or sprays that are widely available for scientific, medical and industrial applications are very popular in mapping temperature fields on surfaces, i.e., for surface tomography applications (Grassi et al. 2007). For natural convection flows however, TLC slurries as a dilute suspension in a carrying fluid are used instead (Fujisawa and Funatani 2000; Stasiek 1997; Stasiek and Kowalewski 2002). A light sheet of white light which cuts a specific cross section of the domain gives a map of the temperature distribution in that sheet. The visualized images have a discrete appearance caused by non-continuous clouds of points. Therefore, some regions of the color images have to be rejected in post-processing if they are too dark (no particle is present in the carrier fluid in a specific area) or if unwanted reflections or light scattering occur.

The TLC calibration has to be performed very carefully in order to obtain an accurate temperature–hue representation for further use in the particle image thermometry (PIT) experiments. The hue–temperature curves are highly nonlinear and depend strongly on the spectral effects of the illumination source, as reported by Anderson and Baughn (2005). In their work, they tested five illumination sources and obtained different color curves which were not all monotonic in the visible range. In this study, we use only one light source to generate a light sheet but with different white balance (WB) color temperatures and we aim to find in this way an optimal setting of the camera in order to capture the most monotonic function of the hue value against the temperature.

As is well known, the three primary colors red (R), green (G) and blue (B) exist in the light source in varying proportions, depending on the color temperature. To human eyes for instance, white objects look always white regardless of the type of lighting. However, for digital CMOS/CCD sensors, the color temperature has to be adjusted so that the color in the image looks more natural. Therefore, a series of experimental measurements have been carried out to test and show the digital camera's response with different WB settings in terms of the color temperatures ranging from 3,000 to 7,000 K. All the tested calibration photographs were shot under the same experimental light conditions; any variation in the light conditions will alter the observed response of the TLC and render the calibration invalid. Different light conditions will require a separate calibration. Although, the topic of the TLCs has been reported in the literature, the current paper addresses certain fundamental but important issues for determining accurate and quantified temperature information not being previously described. It describes some general procedures that can be successfully used with various TLCs and with different optical systems and lighting conditions. It presents step-by-step recipes of the techniques that lead to a proper calibration of the TLC slurries using different camera settings to get the most monotonic color response to temperature. The methods presented below can be used with a range of equipment as a general guide for PIT measurements with many possible applications in science, industry and medicine.

2 Experimental apparatus

A cube of $3 \times 3 \times 3$ cm^3 was used as an enclosure to carry out the calibration experiments. The four sidewalls of the cube were made of transparent Perspex, and the top/bottom walls were made of 3-mm-thick copper plates, which also form parts of the upper and lower cooling chambers as seen in Fig. 1. Water of constant temperature was pumped through the chambers from a circulator controlled by a PC computer. The cube has three holes in one sidewall for mounting thermistors for temperature monitoring. The rear sidewall of the cube was covered by a sheet of non-reflective black paper as a background for experimental photography. The working fluid was inserted into the enclosure through the filling hole using a syringe and a thin needle, and the filling hole in the wall was sealed afterwards by a screw and silicone resin. These procedures have been developed by the authors and co-workers over many years and are reported, for example, in Bednarz et al. (2007, 2008).

A 12.8-MPix CMOS digital camera (EOS 5D) and a lens with 70–200 zoom and aperture f/2.8, covered by a UV filter were used for photography. The camera was placed on a tripod at a distance of 1.5 m from the cube, perpendicular to the front sidewall, and focused on the illuminated plane of liquid crystals. The illumination was from a white light source of a halogen lamp of a slide projector with a color temperature of about 3,000 K. The spectral composition of the light source is unknown; however, so long as the same light source is used in subsequent experiments using this calibration, the composition is immaterial. A thin slit film was placed at the film location of the projector so that a thin light sheet was obtained over a long

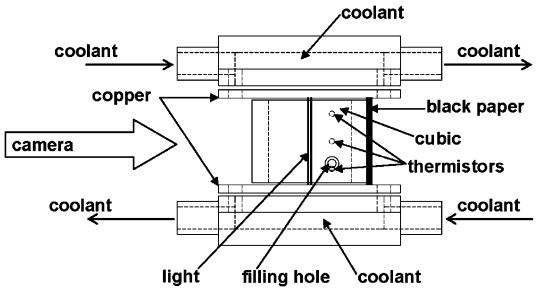

Fig. 1 Experimental apparatus

distance. The position of the illumination source and the viewing angles remained unchanged for all the experiments concerning different WB settings. The purpose of the present investigation was to achieve the most optimal calibration configuration with one light source by manipulating different camera settings. Information about spectral effects of different illumination sources can be found in Anderson and Baughn (2005).

New experimental fluid was prepared for every experimental case: approximately 0.1–0.15 ml of TLC KXN-20/30 (Japan Capsular Products Inc) was mixed with 1 l of distilled water. It is important to keep the TLC concentration the same throughout the calibration. The working fluid is normally clear or slightly milky in appearance, and the TLCs reflect a definite color at a specific temperature. An accurate calibration is required using the HSI color representation so that observed colors can be converted into temperature values.

3 HSI color representation

First, a specification of colors must be defined. The HSI (hue, saturation, intensity) color space has very important features for image processing; it represents colors in a way that is similar to the way that the human eye senses colors. If we have an image in the RGB color format, the H component of each RGB pixel can be obtained using the following equation (Gonzalez et al. 2004):

$$H = \begin{cases} \theta & \text{if } b \le g \\ 360 - \theta & \text{if } b > g \end{cases} \quad \text{where} \quad \theta = \cos^{-1}\left\{ \frac{0.5[2r - g - b]}{\left[(r-g)^2 + (r-b)(g-b)\right]^{0.5}} \right\}.$$

The intensity I and saturation S components can be computed as follows:

$$I = \frac{1}{3}(r + g + b) \quad S = 1 - \frac{\min(r, g, b)}{I}$$

where $r = R/(R + G + B)$, $g = G/(R + G + B)$ and $b = B/(R + G + B)$. The R, G and B represent color components and have values from 0 to 255.

4 Effect of image filtering

Figure 2 shows an example photograph taken during a conduction experiment in the cube heated from above and cooled from below. Linear temperature stratification is established in the cube. The vertical light sheet was cast through the middle-plane of the cube, and the photograph was taken in the plane perpendicular to the front wall. The TLCs responded with the colors belonging to the visible electromagnetic light spectrum depending on the fluid temperature. Due to the finite diameters of the TLC particles, the spatial distribution of the particles in the illuminated plane, and some effects of unwanted reflections, the original photograph has a "sandy" appearance. It can be clearly seen from the enlarged portion of the experimental photograph, in which lighter and darker areas are visible, that discrete TLC particles can be identified. In this case the TLC particles cover approximately 6–10 pixels each (the particle size in pixels can be estimated based on the nominal diameter of the TLCs, the field of view, and the image resolution). An examination of the entire

flow field of interest in Fig. 2 reveals that the upper part of the enclosure has black color areas. The appearance of the black background in the photograph is caused by sedimentation of the TLC particles which cannot be suspended uniformly across the whole flow domain for a very long time. The present conduction experiment took about 4 h to reach a steady state. Usually, convection experiments last for a relatively shorter time, and thus the sedimentation of TLC particles is not an issue. It is strongly recommended that, before carrying out experiments, the working fluid is mixed with the TLC particles using, for instance, a magnetic mixer to get uniform particle concentration across domain. Also, if the fluid is used for multiple experiments, it is desirable to prepare a new one after several experiments since the color response of TLC particles weakens with time.

The experimental photographs need to be post-processed in order to remove or suppress existing pixel noise which has a strong influence on the image quality and the estimation of the color components. In image processing, several noise removal techniques and algorithms are well known. They usually concern techniques with one color component, which is the easiest case to adopt and the most successfully applied in gray-scale image processing. However, in the PIT technique the focus is on color, and it is not a trivial task to adopt noise removal techniques for color images consisting of three separate color components for every single pixel. A simple spatial mean filter is one of the many existing techniques. It is based on a sliding-window analysis that calculates the mean value of each separate color component in the window and replaces the center pixel value with the calculated mean value. The method itself is simple and results in a smooth and clearly averaged image as seen in Fig. 2, for which the analysis was carried out using an 11×11 window size. The mean filter, however, has some disadvantages when compared with a median filter. The median filter is commonly used in image processing due to its spatial noise removal and noise suppression properties. It has also edge-preserving smoothing behavior on the processed images. These features make the median filtering a useful tool for the post-processing of the photographs taken during thermal experiments with TLC particles suspended in a working fluid. These two filters are commonly used in the literature for noise removal from experimental photographs of TLCs (Baughn et al. 1999; Grassi et al. 2007).

The median filter is based on conditional ordering and used as a nonlinear operator to at first arrange the pixels in a local window of a defined radius according to the values of their color components. It then replaces the value of the center pixel in the resulting image by the middle RGB vector from the list. Therefore, with the median filter a very unrepresentative pixel in the neighborhood will not affect the final color vector, and the median filter does not create any new unrealistic pixel values when the filter straddles an edge or when there is a sudden color change. Figure 2 shows the comparison of the two filters described above. Clearly, in the resultant images with both filters, the amount of dark and light shades and noise are substantially reduced, and the images have a smoother appearance. The median filter however, undoubtedly preserves the edge, whereas the mean filter creates an artificial smoothed transition from the region where the fluid meets the side wall, and thus introduces additional uncertainty to the calibration. For the purpose of this paper, a median filter based on conditional ordering is used (Koschan and Abidi 2001).

Figure 3 shows the results of median filtering on an experimental image of water with suspended TLC particles kept at a constant temperature of 20.4°C. The resulting color response of the TLC KXN-20/30 is turquoise with a computed hue value $H = 130$. Different window sizes (5×5, 9×9, 15×15 and 21×21) for median image processing were applied on the input image, and the increasing smoothing effect with the increasing window size is clearly seen in Fig. 3. With the 5×5 window size, the sandy appearance is clearly reduced, and the white pixels caused by unwanted reflections disappear. The image however, still has a grainy appearance. The best smoothing result is noticeably obtained for the window size of 21×21. It is anticipated that increasing the window size further will result in an increasingly smoothed image. However, for applications of median filtering to images taken from a non-uniform temperature field, the

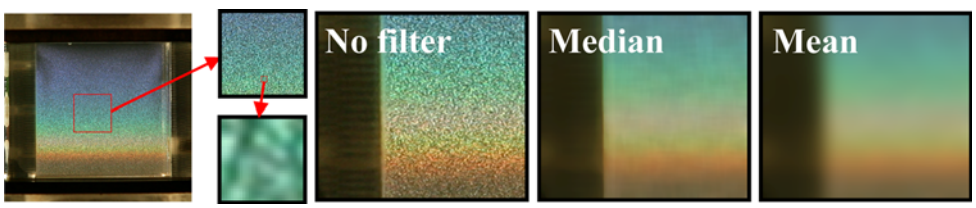

Fig. 2 Photograph taken during conduction experiment: working fluid is heated from above and cooled from below. Also comparison of image processing results: no filter, edge-preserving median filter and mean filter

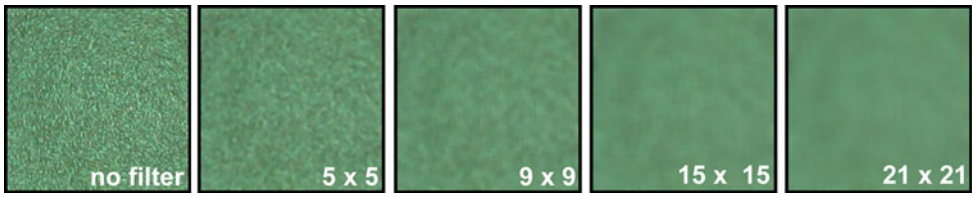

Fig. 3 Effect of the median filtering on the experimental photograph

choice of the window size for correct analysis should be determined with consideration of other aspects such as the resolution of the photograph, the color variations caused by the temperature changes, and the particles' size as will be shown later in this section.

Table 1 gathers corresponding values of mean color components and hue values calculated for the entire experimental domain with the standard deviations listed for each component. For the input image (with no filter), the standard deviations of color components have relatively high value of $\mathrm{SDev_R} = 17.29$, $\mathrm{SDev_G} = 18.50$ and $\mathrm{SDev_B} = 18.23$. The standard deviation of the hue value is much smaller ($\mathrm{SDev_H} = 6.26$). The R, G and B variables take values from 0 up to 255, and the hue value ranges from 0 to 360. Therefore, the variation of the hue values is much smaller when compared to the RGB color components. This behavior can be simply explained with the definition of the hue value which is independent of the saturation and intensity. The application of the median filter on the photograph minimizes the scattering effect while keeping the average hue value of the analyzed window at virtually the same level as seen in Table 1.

An additional test was carried out in order to investigate the effect of median filtering on photographs from a convection experiment in a reservoir model cooled from above (Bednarz et al. 2008). The enclosure for that experiment was made of Perspex and was 0.3 m long, 0.06 m wide and 0.015 m high. Inside the enclosure a slope of inclination 0.1 was fixed to the walls. The enclosure was covered by a copper plate above which the water was constantly pumped from a constant water circulator to cool down the top water surface. Figure 4 shows two photographs taken during two different experiments with different image resolutions. The first image (Fig. 4a) was taken from the same distance as the calibration pictures, and thus has the same particles size (6–10 pixels) as the calibration images. The second image (Fig. 4b) has particle sizes estimated to be around 11–20 pixels. The input images were subject to median filtering of different window sizes. It is seen in Fig. 4 that the increase of the window size caused the images to be more smoothed. As presented above, the increase of the window size reduces the scattering effect; however, a large window size also causes increasing distortion of the color patterns compared with the original image.

The quality of the reconstructed image can be measured by the traditional distortion measures such as peak-signal-to-noise ratio (PSNR) and the mean absolute error (MAE) defined in (Chan et al. 2005; Thakur and Anand 2005):

$$\mathrm{PSNR} = 10\log_{10}\frac{360^2}{\frac{1}{N}\sum_{i,j}\left(r_{i,j}-x_{i,j}\right)^2}; \quad MAE = \frac{1}{N}\sum_{i,j}\left|r_{i,j}-x_{i,j}\right|$$

where N is the number of pixels considered, $r_{i,j}$ and $x_{i,j}$ denote the pixel hue values of the restored image and the original image, respectively.

Figure 5 shows the plots of PSNR and MAE for different window sizes of the median filter for the photographs shown in Fig. 4b. In general, it can be observed, that the MAE increases and PSNR decreases with the window size. There exists a relatively flat region in the MAE and PSNR plots in which the calculated MAE and PSNR values are relatively insensitive to the window size. The flat region corresponds to window sizes of 11×11, 15×15, 19×19. It indicates that, in the relatively flat region, increasing the window size gives a nearly constant hue estimation error (MAE) while reducing the pixel scattering caused by unequal particle distributions. If the window size is increased further beyond the flat region, it can be seen in Fig. 5 that the MAE increases steeply and the quality of reconstructed image (quantified by the PSNR value) is reduced sharply. This is because of the over-smoothing effect of medium filtering with large window sizes.

It is found that the optimal window size approximately corresponds to the particle size. With the first set of images shown in Fig. 4a, the particle size is about 6–10 pixels. A window size between 5×5 and 9×9

Table 1 The red, green, blue and hue values and their standard deviation for the post-processed images presented in Fig. 5

Median	R	$SDev_R$	G	$SDev_G$	B	$SDev_B$	H	$SDev_H$
No filter	100.96	17.29	148.10	18.50	110.25	18.23	130.42	6.26
5 × 5	99.13	6.57	146.23	8.48	108.33	7.924	130.41	5.12
9 × 9	98.89	4.24	145.95	5.62	108.04	5.23	130.46	3.86
15 × 15	98.82	3.15	145.83	4.04	107.96	3.77	130.51	2.88
21 × 21	98.80	2.68	145.83	3.35	107.94	3.14	130.53	2.40

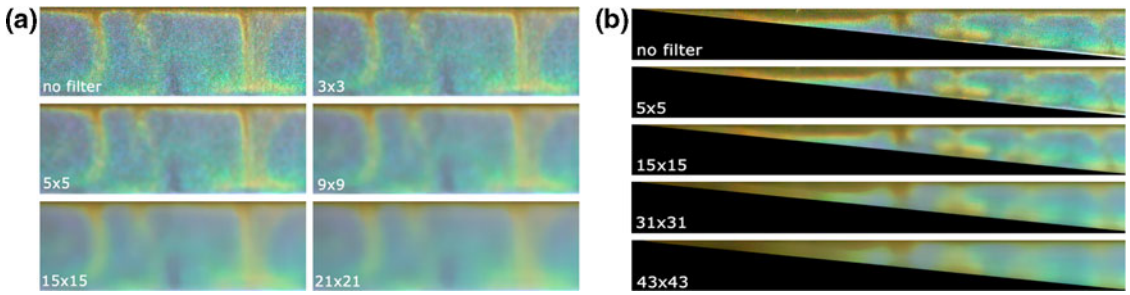

Fig. 4 Sample photographs from two different convection experiments with the estimated particle size in digital images being **a** 6–10 pixels; **b** 11–20 pixels

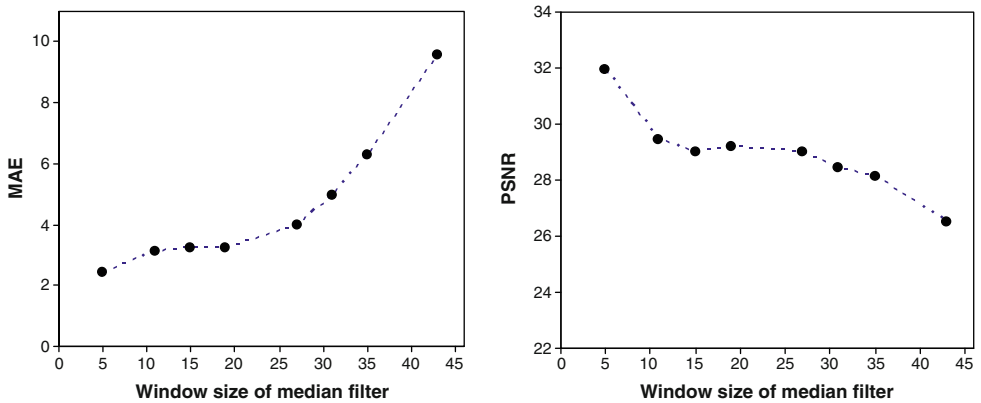

Fig. 5 Results in *PSNR* and *MAE* for the images from Fig. 4b

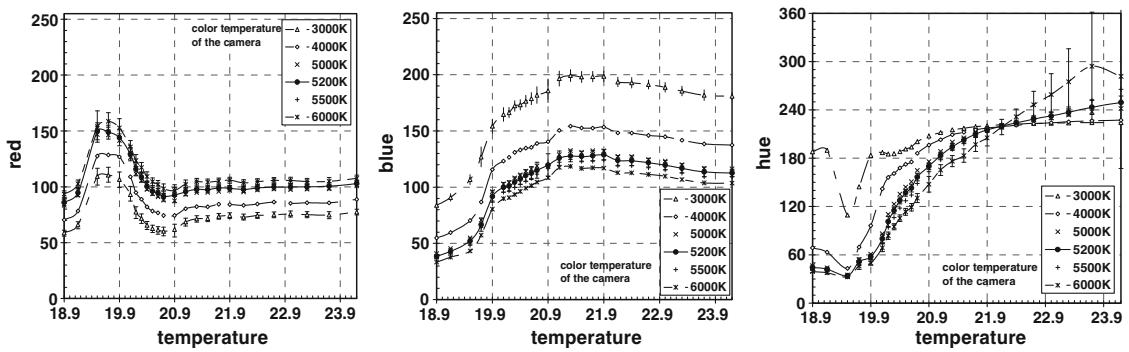

Fig. 6 Response of the TLCs colors in photographs depending on color temperature of the camera used in the experiment: red, blue and hue values. *Error bars* represent standard deviation of hue value at the specific point

will give good results. However a window size of 9 × 9 is preferable due to its greater noise reduction. Similarly, for the second set of images shown in Fig. 4b, which has a particle size of 11–20 pixels, a window size of 19 × 19 gives the best results in terms of the maximum smoothness and the minimum distortion.

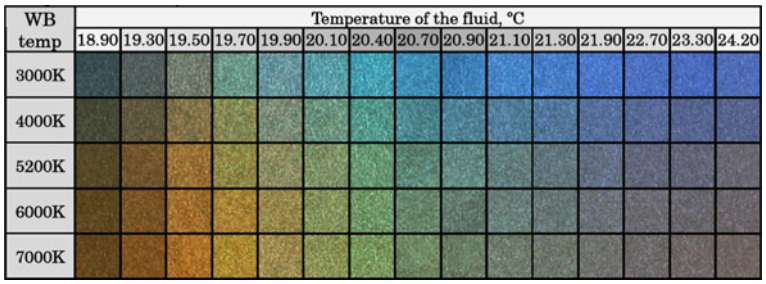

Fig. 7 Color responses of the TLC captured by a digital camera at different fluid temperatures and at different color temperature (*WB*) setting

5 Effect of white balance

The color temperature of digital CMOS sensors must be always adjusted so that the color in the image looks natural. Therefore, several tests were carried out to investigate the digital camera's response with different WB settings in terms of the color temperatures from 3,000 to 7,000 K. All photographs were shot during the experiment in which the water body in the cube was cooled to constant temperatures starting from 24.2°C and finishing at 18.9°C in 26 steps. In every step, the fluid was kept isothermal for about 15–20 min, and experimental photographs were then taken using different settings of the camera. After that, the temperature was set to the lower next calibration point and the above procedure was repeated.

Figure 6 shows the *R*, *B* and corresponding hue values obtained in the calibration experiment with different WB settings. Considering two color components, it can be noted in Fig. 6 that all have definite minima and maxima at specific temperatures. If the color temperature is high, a higher red value is noticeable, and if the color temperature is low, a higher blue value is observed. Moreover, the color temperature of 3,000 K gives a very narrow response of the hue values, and the resulted colors lie in the cold-color region between green and blue. This is seen in Fig. 7, which presents the sampled TLC photographs at different fluid temperatures (18.9–24.2°C) and with different color settings of the camera (3,000–7,000 K). At 3,000 K, all pictures have blue shades, and there are almost no warm colors recognizable. If the color temperature is increased, the blue component decreases, and the red component increases, resulting in warmer color responses.

Considering the temperature–hue plots shown in Fig. 6, it is possible to choose the most monotonic curve of the estimated hues with the highest indicating temperature range. Based on the information obtained during the experiment, the color temperature of 5,200 K was chosen as the best camera setting for further PIT experiments with the present optical system. The experimental photographs obtained at 5,200 K had relatively small values of the standard deviation of the hue compared with other color temperatures as seen in Fig. 6. The obtained temperature–hue curve is monotonic in the range from 19.7 to 23.7°C, which gives approximately 4°C of useful temperature bandwidth for our experimental fluid.

6 Hue–temperature correlation

For the PIT analysis, a correct and accurate hue–temperature correlation is required. The most popular and easiest way is by polynomial regression that fits known temperatures with corresponding hue values calculated from the RGB color components. In the present experiment, a sixth-order polynomial fit is used for the monotonic hue–temperature response region (for temperatures 19.7–23.7°C). Figure 8 shows some sample test results. The target temperature in Fig. 8a is compared with the temperature obtained using the estimated hue–temperature curve. The dashed line denotes the ideal correspondence between the target temperature and the measured temperature. The accuracy of the curve-fitting is assessed by the coefficient of determination R^2 which is 0.9962, and the mean absolute error which is estimated to be 0.0493°C in this case. The correlation obtained by this method is very good.

The polynomial fitting is not the only technique that can be successfully used to convert colors into temperature values. An alternative technique, which may have some advantages over the polynomial curve-fitting described above, is to use trained back-propagation neural networks (Grewal et al. 2006). In particular, it may have additional advantages for the hue–temperature calibration as more than one input

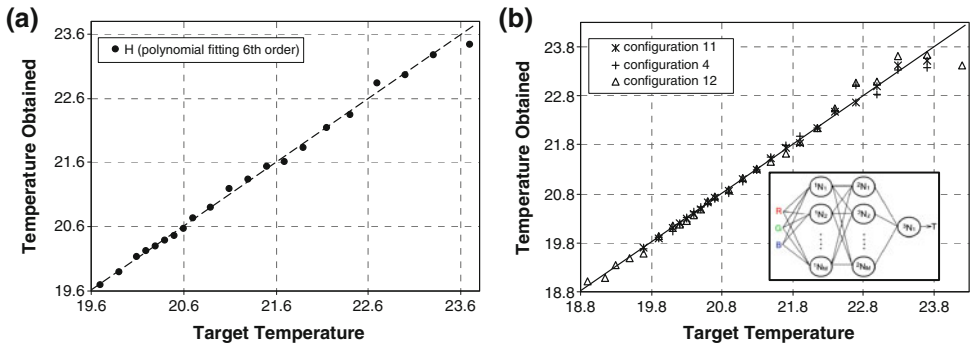

Fig. 8 Target temperature versus temperature obtained using **a** 6th order polynomial fitting, **b** neural networks

parameter is used for estimating the temperature of a pixel. Therefore, several neural network configurations were tested here to compare their performances with each other and with the conventional polynomial curve-fitting technique.

Figure 8b shows a sample neural network configuration for the PIT application with three layers of neurons: the first two have variable numbers of working neurons; and the third one has only one neuron with three inputs and one output. In the test, the input has either three (R, G, B) or four (R, G, B, H) parameters. The networks are trained using the color components curves from the calibration experiment as training vectors, and the measured temperatures as target vectors. The standard back-propagation algorithm (Tadeusiewicz 1993) is used to modify the weights and biases of each network nodes until the root-mean sum of the difference between the calculated and perfect values of target vectors is minimized to a required level. In addition, different activation functions on each layer are tested in order to achieve the best results. The various cases tested are listed in Table 2. For instance, Case 2 has three input parameters with six neurons in the first and second layers and one in the third layer. The hyperbolic tangent sigmoid activation function is used for the first two layers and the log sigmoid activation function is used for the third layer. The analyzed temperatures are limited to the monotonic region of the hue function (the usable TLC color range). Around 10,000 iterations are required to train the neural network to achieve very good level of fitting accuracy. The obtained regression coefficient for Case 2 is $R^2 = 0.9940$ with a mean absolute error of the predicted temperature equal to 0.0545°C. Changing the number of neurons and activation functions for the neural network layers leads to different results. Table 2 compares the performance of different calibration tests carried out using multi-layered multi-input feed-forward back-propagation neural networks along with the sixth-order polynomial curve-fitting. It is found that the mean absolute error can be improved depending on the specific configuration of the neurons and the activation functions adopted. Quite good results are obtained for Case 7, for which the number of neurons on the first and the second layer are reduced to 3, and only log sigmoid activation function is used. The mean absolute error is reduced to 0.0462°C. By increasing the number of inputs from three to four (R, G, B and H), the measurement accuracy is even further

Table 2 Performance of different neural network configurations

No	Input parameters	Neurons in layers	Activation functions	Color bandwidth (°C)	Regression coefficient	Mean absolute error (°C)
1	H	Polynomial fit		19.7–23.7	0.9962	0.0493
2	R, G, B	6, 6, 1	tan, tan, log	19.7–23.7	0.9940	0.0545
3	R, G, B	6, 6, 1	tan, tan, lin	19.7–23.7	0.9949	0.0528
4	R, G, B	6, 6, 1	log, log, lin	19.7–23.7	0.9898	0.0733
5	R, G, B	6, 6, 1	log, log, log	19.7–23.7	0.9952	0.0486
6	R, G, B	2, 2, 1	log, log, log	19.7–23.7	0.9949	0.0493
7	R, G, B	3, 3, 1	log, log, log	19.7–23.7	0.9953	0.0462
8	R, G, B	10, 10, 1	log, log, log	19.7–23.7	0.9943	0.0479
9	R, G, B	20, 20, 1	log, log, log	19.7–23.7	0.9949	0.0456
10	R, G, B, H	3, 3, 1	log, log, log	19.7–23.7	0.9977	0.0375
11	R, G, B, H	20, 20, 1	log, log, log	19.7–23.7	0.9978	0.0319
12	R, G, B	3, 3, 1	log, log, log	18.9–24.2	0.9810	0.1129
13	R, G, B, H	3, 3, 1	log, log, log	18.9–24.2	0.9821	0.1027

Activation functions: log–log sigmoid activation function
lin linear activation function, *tan* hyperbolic tangent activation function

improved. The best results are obtained for Case 11, for which the mean absolute error is only 0.0319°C and $R^2 = 0.9978$. Good accuracy is also obtained for Case 10, for which the number of neutrons is 3 in the first two layers. Case 10 needs less computational time than Case 11 due to the reduced number of neurons. Cases 12 and 13 consider an extended color bandwidth. It is shown that it is possible to get results in an extended range using neural networks with a slight sacrifice of the accuracy. The mean absolute error for those two cases is greater than 0.1°C. Figure 8b shows the comparison of the results for Cases 4, 11 and 12. The straight line denotes the ideal correlation between the target and the expected outputs. Based on Table 2, the best accuracy is achieved in Case 11.

It must be emphasized however that the use of neural networks to evaluate the calibration curve is not a primary goal of this paper. It has been introduced here in a simple way to demonstrate that it may have some advantages over polynomial fitting rather than an exhaustive investigation of the ability of neural networks to complete the calibration.

7 Conclusions

The present paper is concerned with various aspects relevant to quantitative temperature measurements using the PIT technique based on TLC images. At first, the benefits of median filtering for noise removal and edge preserving have been demonstrated. It is shown that the accuracy can be improved with the application of median filtering. The analysis has shown that the optimal window size for median filtering approximately corresponds to the particle size measured in pixels.

The essence of PIT measurements is to obtain a monotonic relation between the hue and the temperature. Using different cameras, different TLCs and different light sources, different temperature–hue pairs are obtained. General procedures described in this paper can be applied to any kind of CCD/CMOS cameras and different types of TLCs. It has been demonstrated that a WB of our camera corresponding to a color temperature of 5,200 K gives the best results. It should be emphasized that every camera system may have different color sensitivity, and the optimum WB color setting may be different to 5,200 K. Therefore, careful calibration should be carried out for a specific experimental condition.

Finally, a series of sample calibration tests were presented. A polynomial curve-fitting is compared with the results obtained from trained neural networks of different configurations. It is found that three layered networks give very accurate fitting results. It is shown that more accurate results are obtained when the networks have four inputs (R, G, B and H) with the log sigmoid activation functions at all layers. Therefore, such three layered neural networks can be successfully used as an alternative approach to the conventional polynomial-fitting technique.

References

Anderson MR, Baughn JW (2004) Hysteresis in liquid crystal thermography. J Heat Transf 126:339–346
Anderson MR, Baughn JW (2005) Liquid-crystal thermography: illumination spectral effects. Part 1—experiments. J Heat Transf 127:591–598
Baughn JW, Anderson MR, Mayhew JE, Wolf JD (1999) Hysteresis and uncertainty of thermo-chromic liquid crystals temperature measurement based on hue. J Heat Transf 121:1067–1072
Bednarz T, Lei C, Patterson JC (2007) Particle image thermometry for natural convection flows. In: Proc. 16th Australasian fluid mechanics conference. pp 1165–1170
Bednarz T, Lei C, Patterson JC (2008) An experimental study of unsteady natural convection in a reservoir model cooled from the water surface. Exp Thermal Fluid Sci 32:844–856
Chan RH, Chuang-Wa H, Nikolova M (2005) Salt-and-pepper noise removal by median-type noise detectors and detail-preserving regularization. Image Process IEEE Trans 14:1479–1485
Fujisawa N, Funatani S (2000) Simultaneous measurement of temperature and velocity in a turbulent thermal convection by the extended range scanning liquid crystal visualization technique. Exp Fluids (Suppl)158–165
Gonzalez RC, Woods RE, Eddins SL (2004) Digital image processing using Matlab, Pearson Education Inc, Prentice Hall
Grassi W, Testi D, Della Vista D, Torelli G (2007) Calibration of a sheet of thermosensitive liquid crystals viewed non-orthogonally. Measurement 40:898–903
Grewal GS, Bharara M, Cobb JE, Dubey VN, Claremont DJ (2006) A novel approach to thermochromic liquid crystal calibration using neural networks. Meas Sci Tech 17:1918–1924
Koschan A, Abidi MA (2001) A comparison of median filter techniques for noise removal in color images. In: Proc. 7th German workshop on color image processing. pp 69–79
Park HG, Dabiri D, Gharib M (2001) Digital particle image velocimetry/thermometry and application to the wake of heated circular cylinder. Exp Fluids 30:327–338

Smith CR, Sabatino DR, Praisner TJ (2001) Temperature sensing with thermochromic liquid crystals. Exp Fluids 30:190–201
Stasiek JA (1997) Thermochromic liquid crystals and true color image processing in heat transfer and fluid-flow research. Heat Mass Transf 33:27–39
Stasiek JA, Kowalewski TA (2002) Thermochromic liquid crystals applied for heat transfer research. Opto-Electron Rev 10:1–10
Tadeusiewicz R (1993) Neural networks (Sieci Neuronowe), Akademicka Oficyna Wydawnicza RM, Warsaw (in Polish)
Thakur A, Anand RS (2005) Image quality based comparative evaluation of wavelet filters in ultrasound speckle reduction. Digit Signal Process 15:445–465